Structures and energetics of Bi_2O_3 polymorphs in a defective fluorite family derived by systematic first-principles lattice dynamics calculations

Akifumi Matsumoto,[1,*] Yukinori Koyama,[1,†] and Isao Tanaka[1,2,‡]
[1]*Department of Materials Science and Engineering, Kyoto University, Kyoto 606-8501, Japan*
[2]*Nanostructures Research Laboratory, Japan Fine Ceramics Center, Nagoya 456-8587, Japan*
(Received 23 November 2009; revised manuscript received 13 January 2010; published 29 March 2010)

A series of dynamically stable structures of the defective fluorite-Bi_2O_3 is found by first-principles lattice dynamics calculations. The crystal symmetry is lowered and local distortion is included systematically along imaginary modes of lattice vibrations. A clear band gap appears when local distortion is included in this way, which is consistent with experimental results. Many theoretical calculations in the past indicated metallic or semimetallic electronic structures. The appropriate inclusion of the symmetry breaking and local distortion are therefore essential in reproducing the electronic structures of Bi_2O_3. The three stable structures are found to have an energy of 0.07–0.08 eV/f.u. relative to α-Bi_2O_3. The arrays of oxide-ion vacancies in two of these structures are the same as those of β-Bi_2O_3 and ε-Bi_2O_3, which were experimentally identified as stable phases. A bixbyite-type vacancy-array structure is also found to be another stable phase in the present study, which is named η-Bi_2O_3. It is suggested that the three stable structures of Bi_2O_3 are ordered low-temperature polymorphs of the disordered δ-Bi_2O_3 in the defective fluorite-Bi_2O_3 family.

DOI: 10.1103/PhysRevB.81.094117 PACS number(s): 61.50.Ah, 63.20.−e, 71.20.−b

I. INTRODUCTION

Bismuth oxide, Bi_2O_3, has been reported to exhibit six polymorphs, α, β, γ, δ, ε, and ω phases.[1–10] α-Bi_2O_3 has a monoclinic structure and is stable at room temperature and atmospheric pressure. It is transformed to δ-Bi_2O_3 upon heating to above 1000 K, which is stable up to its melting point.[1–8] β-Bi_2O_3 and γ-Bi_2O_3 are obtained as metastable phases during the cooling of δ-Bi_2O_3.[1,2,5–7] ε-Bi_2O_3 can be obtained by hydrothermal treatment in highly concentrated KOH solution,[9] and which is irreversibly transformed to the α form at 673 K. ω-Bi_2O_3 has been prepared on a BeO substrate.[10] Since the high-temperature phase, δ-Bi_2O_3, exhibits high oxide ionic conductivity of more than 1 S/cm,[11] it has attracted considerable attention. δ-Bi_2O_3 was reported to have a defective fluorite structure: Bi ions occupy the 4*a* sites at (0, 0, 0), forming a face-centered-cubic sublattice, and oxide ions occupy the 8*c* sites at (1/4, 1/4, 1/4), forming a simple cubic sublattice. Since the Bi ions are trivalent, a quarter of the O sites are vacant to ensure charge neutrality. This high concentration of intrinsic vacant sites provides a simple explanation for the high conductivity of the oxide ions. Therefore, numerous experimental and computational studies have been performed on the arrangement of oxide ions and vacant sites in the O sublattice.[3,4,12–23] Sillen suggested that the vacant sites were ordered along the ⟨111⟩ direction on the basis of powder x-ray diffraction measurements on quenched samples.[3] Gattow and Schröder reported that no ordering was observed in the O sublattice upon performing high-temperature powder x-ray diffraction.[4] Since then, the arrangement of vacant sites has been assumed to be random. Also, the oxide ions were reported to be off-centered from the ideal sites in the fluorite structure according to recent neutron-diffraction experiments.[12,13]

To elucidate the structure of δ-Bi_2O_3 and the nature of its high ionic conductivity by theoretical approaches, several studies using first-principles calculations based on density-functional theory (DFT) have been reported.[14–23] A unit cell of the simplest defective fluorite structure contains eight O sites, of which two are vacant. In the present study, this unit cell will be hereafter referred to as the single unit cell. The term "array" will be used to distinguish the arrangement of vacancy sites in the O sublattice. There are three possible arrays of the vacant sites in the single unit cell. They are aligned along either the ⟨100⟩, ⟨110⟩, or ⟨111⟩ direction, as schematically shown in Fig. 1. Displacements from the ideal exact atomic positions are introduced to lower the symmetry from that of the cubic fluorite structure. This will be referred as "symmetry breaking." Symmetry breaking is accompanied by a set of local distortion. The number of different atomic arrangements for a given vacancy array increases with the lowering of the symmetry. However, all the different variations induced by symmetry breaking on the same idealized structure are included in the same array. In this study, the term "arrangement" will retain its general meaning and refer to a set of specific atomic positions.

Theoretical calculations on defective fluorite Bi_2O_3 (df-Bi_2O_3) with the three different vacancy arrays formed for the single unit cell have been performed in many studies. In these studies, δ-Bi_2O_3 was approximated by these simplified df-Bi_2O_3 models. No procedure to statistically treat the dis-

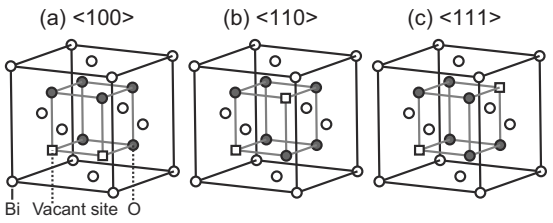

FIG. 1. Three possible arrays of the vacant sites in a single unit cell aligned along the (a) ⟨100⟩, (b) ⟨110⟩, and (c) ⟨111⟩ directions. White spheres, gray spheres, and white squares denote Bi, O, and vacant sites, respectively.

ordered phase was included. Information by these simplified model calculations is therefore limited. In order to highlight the limitation of these models, we use the term δ-Bi_2O_3 exclusively for the high-temperature phase in the present paper.

Medvedeva *et al.*[14] first reported first-principles calculations of df-Bi_2O_3 using the linear muffin-tin orbital method with the local-density approximation. They suggested that an arrangement in the ⟨111⟩ array (a ⟨111⟩ arrangement) had a metallic electronic structure and was more stable than a ⟨110⟩ arrangement. Carlsson *et al.*[15] reported first-principles calculations of α-Bi_2O_3 and df-Bi_2O_3 using the plane-wave basis ultrasoft-pseudopotential method with the generalized-gradient approximation (GGA). They suggested that a ⟨100⟩ arrangement was the most stable among the three arrangements with different vacancy arrays, and that its energy was 0.80 eV/f.u. (f.u.: formula unit) higher than that of α-Bi_2O_3. In the electronic structure of the ⟨100⟩ arrangement, the top of the valence band had a higher energy than the bottom of the conduction band, indicating a semimetallic electronic structure. Walsh *et al.*[16] also reported similar results for first-principles calculations using the projector augmented wave (PAW) method with the GGA. Their ⟨100⟩ and ⟨110⟩ arrangements were semimetallic while the ⟨111⟩ arrangement was metallic. The ⟨100⟩ arrangement was the most stable among the three arrangements and had a higher energy than α-Bi_2O_3 by 0.74 eV/f.u. Experimentally, δ-Bi_2O_3 exhibits a clear band gap of 1.73 eV.[24] Since this was obtained in a nanocrystalline thin-film sample, the band gap of the perfect crystalline δ-Bi_2O_3 may be larger than 1.73 eV. However, all the above calculations indicated semimetallic or metallic electronic structures. Zhong *et al.*[20] considered spin-orbit coupling as a relativistic effect in the Bi ions using the full-potential linearized augmented plane-wave method with the GGA. They reported that a ⟨110⟩ arrangement had a band gap of 0.46 eV and was the most stable among the three arrangements. They suggested that the spin-orbit coupling effect was an important factor in determining the size of the band gap. However, their ⟨111⟩ arrangement was still metallic.

Recently, calculations on df-Bi_2O_3 beyond the single unit cell, i.e., the df-Bi_2O_3 superstructure have been reported. Aidhy *et al.*[17] found an arrangement having lower energy than those in the single-unit-cell models when a $2\times2\times2$ superstructure was examined by a combination of classical molecular-dynamics (MD) simulations and PAW calculations with the GGA. Music *et al.*[21] reported that some arrangements of the $2\times2\times2$ superstructure were lower in energy than the ⟨100⟩ arrangement using the ultrasoft-pseudopotential method with the GGA. They confirmed that the arrangement reported by Aidhy *et al.* was the lowest in energy. Mohn *et al.*[22,23] reported that there were many arrangements of the $2\times2\times2$ superstructure lower in energy than the three single-unit-cell models on the basis of first-principles MD simulations and lattice statics calculations combined with powder neutron-diffraction experiments. They suggested that the distribution of the oxide ions surrounding the Bi ions was highly asymmetric.

In spite of these extensive studies, two major issues remain. (1) The electronic structure, particularly the band gap, is inconsistent with experimental results; the three simple arrangements within the single unit cell are semimetallic or metallic. The experimentally obtained band gap of δ-Bi_2O_3 is 1.73 eV.[24] (2) The theoretical energy of df-Bi_2O_3 relative to α-Bi_2O_3 has not been conclusively determined. Both Carlsson *et al.* and Walsh *et al.* reported that their ⟨100⟩ arrangement is ~0.7 eV/f.u. higher in energy than α-Bi_2O_3. Using superstructure models, Mohn *et al.*[23] recently reported the presence of low-energy structures that are more than 0.13 eV/f.u. higher in energy than α-Bi_2O_3. As will be shown later, these structures are not the lowest-energy arrangements within the given array.

Carlsson *et al.* performed a series of first-principles calculations to examine the energy barrier of df-Bi_2O_3 between ⟨111⟩ and ⟨100⟩ arrangements via a ⟨110⟩ arrangement by displacing an oxide ion. They found no energy barrier for the transformation from ⟨111⟩ to ⟨110⟩. Although the result is not quantitatively reliable since they did not include the probable relaxation of the structure during the transformation, it appears that the ⟨111⟩ arrangement is not stable against lattice dynamics. Therefore, we investigate the lattice dynamics of each structure. In this paper, we will show that the reported structures are dynamically unstable and that symmetry breaking and local distortion around Bi ions are essential for describing the atomic and electronic structures of Bi_2O_3 with a defective fluorite structure. The local distortion leads to a wide band gap of 2–3 eV. It also considerably reduces the energy even though the array is not changed. The lowest energy relative to α-Bi_2O_3 is found to be 0.07–0.08 eV/f.u. We show three different examples of such low-energy structures, all of which are stable with respect to the lattice dynamics.

II. COMPUTATIONAL PROCEDURES

The first-principles calculations were performed by the PAW method[25] implemented in the VASP code.[26–28] Plane waves were used as the basis functions with a cutoff energy of 360 eV. The convergence of the formation energy with respect to the plane-wave cutoff was found to be better than 0.01 eV/f.u. The radii of the PAW potentials were 1.32 and 0.98 Å for Bi and O, respectively. The 5*d*, 6*s*, and 6*p* electrons for Bi and the 2*s* and 2*p* electrons for O were treated as valence and the remaining electrons were kept frozen. The exchange-correlation term was treated with the Perdew-Burke-Ernzerhof functional based on the GGA.[29] Both the unit cell of the fluorite structure and the $2\times2\times2$ supercell were used for df-Bi_2O_3. Integration in the reciprocal space was performed by the Monkhorst-Pack scheme using a $4\times4\times4$ mesh for the single unit cell, a $2\times2\times2$ mesh for the $2\times2\times2$ supercell and a $3\times2\times2$ mesh for α-Bi_2O_3. The total energy was minimized until the energy convergence became less than 5×10^{-6} eV/f.u. The stability of the model structures against lattice dynamics was examined as described in the following sections. The force-constant approach involving a finite displacement was used for this purpose by employing the fropho code.[30–32] The $2\times2\times2$ supercells were used with a displacement of 0.01 Å along the *x*, *y*, and *z* directions for each atom.

TABLE I. Details of calculated structure, Bi-O bond length, and band gap of α-Bi_2O_3. The values in parenthesis were obtained from experiments (Refs. 32 and 33).

			α-Bi_2O_3			
Space group			$P2_1/c$ (No. 14)			
Lattice parameter			a=5.93 Å (5.84 Å) b=8.28 Å (8.15 Å) c=7.54 Å (7.50 Å) β=113° (113°)			
Atom coordinate	Bi (1)	4e	0.524	0.184	0.366	(0.523 0.184 0.362)
	Bi (2)	4e	0.040	0.041	0.777	(0.040 0.043 0.776)
	O (1)	4e	0.778	0.298	0.707	(0.777 0.304 0.707)
	O (2)	4e	0.235	0.052	0.125	(0.235 0.048 0.127)
	O (3)	4e	0.270	0.031	0.512	(0.269 0.028 0.511)
Bond length (Å)			Bi(1)-O(1)			2.24×1
						2.58×1
			Bi(1)-O(2)			2.21×1
			Bi(1)-O(3)			2.12×1
						2.50×1
			Bi(2)-O(1)			2.23×1
						2.53×1
			Bi(2)-O(2)			2.15×1
						2.41×1
			Bi(2)-O(3)			2.29×1
						2.80×1
Band gap (eV)			2.29 (2.5)			

III. RESULTS

A. α-Bi_2O_3 and the three arrangements within the single unit cell for df-Bi_2O_3

α-Bi_2O_3 and the three arrangements of Bi_2O_3 with the single unit cell are examined in this section. Their atomic and electronic structures are described with a review of similar works in the literature.[14–16] The optimized structure of α-Bi_2O_3 is summarized in Table I. The lattice constants and internal positions are in good agreement with experimental results.[33] α-Bi_2O_3 exhibits the electronic band structure shown in Fig. 2 with a band gap of 2.29 eV. The gap is 0.2 eV smaller than that obtained by experiments.[34] This underestimation is within the expected range of the GGA error. The three arrangements for df-Bi_2O_3 were constructed simply by locating the Bi and oxide ions in the ideal positions of the fluorite structure, and the structures were optimized while maintaining the initial symmetry. The symmetry, optimized structural data, and energy relative to α-Bi_2O_3 are summarized in Table II. The electronic band structures are illustrated in Fig. 3. The ⟨100⟩ arrangement has the lowest energy among the three arrangements. However, it has a higher energy than α-Bi_2O_3 by 0.73 eV/f.u. The energy difference among the three arrangements and α-Bi_2O_3 is in quantitatively good agreement with those in the literature.[16] Both the ⟨100⟩ and ⟨110⟩ arrangements have a gap between the valence and conduction bands. However, the valence-band tops are above the conduction-band bottoms. Hence, these two arrangements are semimetallic. In contrast, the Fermi energy intersects the bands in the ⟨111⟩ arrangement, indicating that the ⟨111⟩ arrangement is metallic.

Lattice dynamics calculations are performed on the three arrangements. Figure 4 illustrates the phonon band structures of the ⟨100⟩, ⟨110⟩, and ⟨111⟩ arrangements computed in the present study. Note that the phonon dispersion curves are shown with the notation of the wave vectors in the corresponding unit cells since each arrangement has a different symmetry and size of the unit cell. The imaginary value of

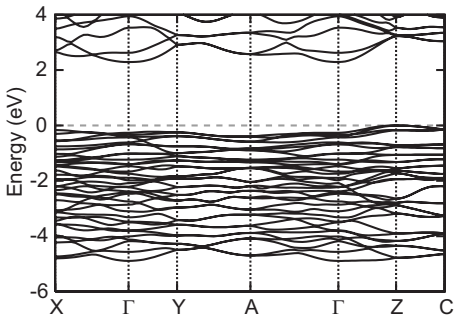

FIG. 2. Electronic band structure of α-Bi_2O_3. The top of the valence band is set to 0 on the vertical axis.

TABLE II. Details of structure, Bi-O bond length, and energy relative to α-Bi_2O_3 of the three arrangements in the single unit cell for df-Bi_2O_3.

	⟨100⟩					⟨110⟩					⟨111⟩				
Space group	$P4_2/mcm$ (No. 132)					$P\bar{4}m2$ (No. 115)					$Pn\bar{3}m$ (No. 224)				
Lattice parameter	a=5.84 Å c=5.72 Å					a=3.92 Å ($\sqrt{2}a$=5.54 Å) c=5.85 Å					a=5.59 Å				
Atom coordinate	Bi (1)	4*i*	0.736	0.736	0	Bi (1)	2*g*	0	0.5	0.777	Bi (1)	4*b*	0.25	0.25	0.25
	O (1)	4*e*	0	0.5	0.25	O (1)	1*a*	0	0	0	O (1)	6*d*	0	0.5	0.5
	O (2)	2*d*	0.5	0.5	0.25	O (2)	1*b*	0.5	0.5	0					
						O (3)	1*d*	0	0	0.5					
Bond length (Å)	Bi(1)-O(1)		2.42×2			Bi(1)-O(1)		2.35×2			Bi(1)-O(1)		2.42×6		
	Bi(1)-O(2)		2.51×4			Bi(1)-O(2)		2.35×2							
						Bi(1)-O(3)		2.54×2							
Relative energy (eV/f.u.)	0.73					0.85					1.85				

the frequency illustrated below 0 indicates that the structure is at a local maximum of the potential surface and is unstable against the corresponding lattice vibration. All three arrangements have vibration modes with imaginary frequency at any point in the first Brillouin zone (BZ).

B. Symmetry breaking and local distortion in ⟨111⟩ array model

In this section, we investigate the dynamically stable structure of the ⟨111⟩ vacancy-array model, which exhibits a metallic electronic structure and the highest energy, as described in the previous section. First, a new structure is constructed by introducing a displacement of ~0.5 Å along the eigenvector of the imaginary vibration mode at the Γ point (0, 0, 0) in Fig. 4(c). The set of atomic displacements is schematically shown in Fig. 5. This is the set of displacements that can be included in the single unit cell. As will be shown later, the description of the set of displacements corresponding to the other points in the BZ such as the R point (1/2, 1/2, 1/2) requires the use of a supercell. The structural parameters are optimized after introducing the set of displacements. Note that both the new arrangement and the original arrangement are included in the ⟨111⟩ array model. However, the symmetry is lower in the new arrangement. We will hereafter call the original and new arrangements the high-symmetry (HS) and low-symmetry (LS) arrangements, respectively.

The displacement in the ⟨111⟩-HS arrangement leads to *R*3*m* space-group symmetry. The optimized structural data of the ⟨111⟩-LS arrangement is summarized in Table III. The symmetry breaking causes a local distortion around Bi ions. The Bi-O bond length is constant at 2.42 Å in the HS arrangement, whereas it varies in the range of 2.14–3.07 Å in the LS arrangement. This variation in the Bi-O bond length should be preferred by Bi^{3+}, since α-Bi_2O_3 also has a variable bond length, ranging from 2.12 to 2.80 Å. The symmetry breaking and local distortion leads to a marked change in the electronic structure. Figure 6 illustrates the electronic band structure of the ⟨111⟩-LS arrangement. There is a band gap of 2.37 eV, which is in strong contrast to the metallic structure of the ⟨111⟩-HS arrangement shown in Fig. 3(c). The ⟨111⟩-LS arrangement is lower in energy than the ⟨111⟩-HS arrangement by 1.46 eV/f.u. These results imply that the inclusion of the symmetry breaking and local distortion is essential to describe the atomic and electronic structures of df-Bi_2O_3. The constraint of imposing too high symmetry should lead to an incorrect electronic structure with too high energy. Although the energy of the ⟨111⟩-LS arrangement is significantly lower than that of the ⟨111⟩-HS

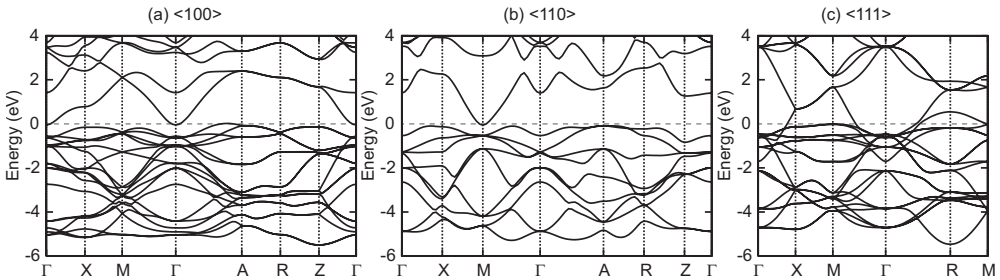

FIG. 3. Electronic band structures of the three arrangements in the single unit cell for df-Bi_2O_3 shown in Table II. The top of the valence band is set to 0 on the vertical axis.

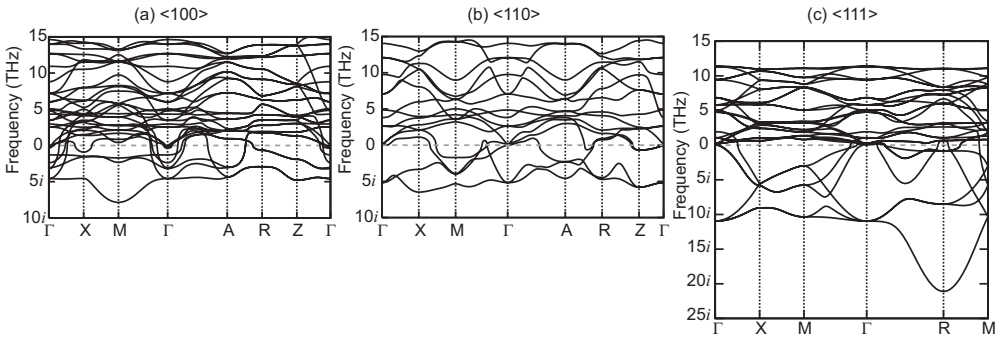

FIG. 4. Phonon band structures of the three arrangements in the single unit cell for df-Bi_2O_3 shown in Table II.

arrangement, an additional phonon calculation for the ⟨111⟩-LS arrangement found that a small imaginary frequency remains at the L point (1/2, 0, 1/2) of the unit cell of the ⟨111⟩-LS arrangement, which corresponds to the X point (1/2, 0, 0) in the notation of the original primitive cell shown in Fig. 4(c). This implies that the current ⟨111⟩-LS arrangement is not a dynamically stable structure.

To examine wave vectors other than the Γ point in Fig. 4(c), we need to construct supercell models. The supercells will hereafter be denoted by their sizes compared with the single unit cell. Since we employed the $2\times2\times2$ supercell for the phonon calculations, we considered only the wave vectors commensurate with the periodicity of the supercell. These wave vectors will be hereafter referred to as "commensurate points." Atomic displacements that correspond to the imaginary vibration mode having the largest absolute value (or the strongest imaginary frequency) are chosen. For the ⟨111⟩-HS arrangement, the strongest imaginary frequency appears at the R point (1/2, 1/2, 1/2) in Fig. 4(c), and the new arrangement requires a $2\times2\times2$ supercell as the unit cell. The displacement leads to a structure with the space group $Fd\bar{3}m$. The structure is optimized by imposing the $Fd\bar{3}m$ symmetry. We will hereafter call the newer arrangement the ⟨111⟩-LS($2\times2\times2$) arrangement, whose structural data is summarized in Table IV. Interestingly, the ⟨111⟩-LS($2\times2\times2$) arrangement is isostructural to arsenolite, As_2O_3, and senarmontite, Sb_2O_3. Its band gap is 2.59 eV, which is larger than that of the ⟨111⟩-LS arrangement. The ⟨111⟩-LS($2\times2\times2$) arrangement is lower in energy than the ⟨111⟩-LS arrangement by 0.10 eV/f.u. It does not exhibit dynamical instabilities at the commensurate points according to the results of phonon calculations. In the following section, however, we will see that there are more stable arrangements of df-Bi_2O_3 than the ⟨111⟩-LS($2\times2\times2$) arrangement.

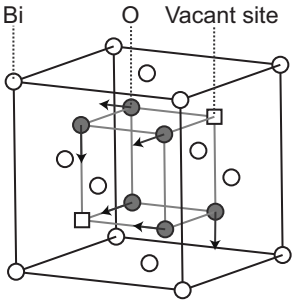

FIG. 5. Schema of the eigenvectors of the imaginary vibration mode at the Γ point (0,0,0) in the ⟨111⟩ model [see also Fig. 4(c)]. The displacement of Bi atoms is much less than that of O atoms. The directions of the vibration of O atoms are almost parallel to the Cartesian axes.

C. Symmetry breaking and local distortion in ⟨100⟩ array model

Symmetry breaking in the ⟨100⟩ array model is also examined within the $2\times2\times2$ supercell. Similar to the case of the ⟨111⟩-LS($2\times2\times2$) model, a set of atomic displacements is initially made toward the eigenvector of the strongest imaginary frequency. The displacements correspond to the M point (1/2, 1/2, 0) in Fig. 4(a), which leads to the structure of the space group $P4_2/nmc$ with a $\sqrt{2}\times\sqrt{2}\times1$ supercell as the unit cell. After the structure optimization with the space group $P4_2/nmc$, a weak imaginary frequency remains at the Γ point (0, 0, 0). Optimization eventually leads to the ⟨100⟩-LS($2\times2\times2$) arrangement with the space group $P\bar{4}2_1c$, which does not exhibit dynamical instabilities at the commensurate points. The structural data, Bi-O bond length, band gap and energy relative to α-Bi_2O_3 for this arrangement are summarized in Table V. The relative energy of the ⟨100⟩-LS($2\times2\times2$) arrangement is only 0.08 eV/f.u. It is very interesting that the ⟨100⟩-LS($2\times2\times2$) arrangement obtained in this way is isostructural to the experimentally ob-

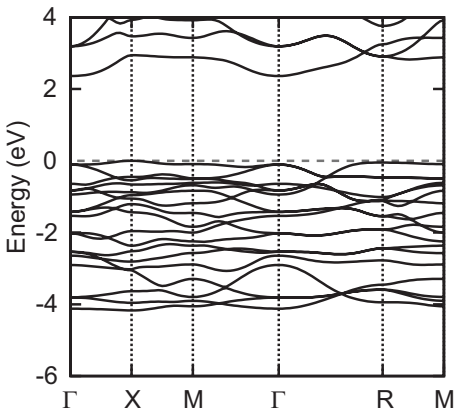

FIG. 6. Electronic band structure of ⟨111⟩-LS arrangement of df-Bi_2O_3 shown in Table III. The top of the valence band is set to 0 on the vertical axis.

TABLE III. Details of structure, Bi-O bond length, energy relative to α-Bi_2O_3, and band gap of ⟨111⟩-LS arrangement of df-Bi_2O_3.

			⟨111⟩-LS		
Space group			*R*3*m* (No. 160)		
Lattice parameter			a=5.78 Å α=88.8°		
Atom coordinate	Bi (1)	3*b*	0.522	0.030	0.522
	Bi (2)	1*a*	0.000	0.000	0.000
	O (1)	3*b*	0.265	0.656	0.265
	O (2)	3*b*	0.763	0.158	0.763
Bond length (Å)		Bi(1)-O(1)		2.14×2	
				3.07×1	
		Bi(1)-O(2)		2.15×1	
				2.95×2	
		Bi(2)-O(1)		2.92×3	
		Bi(2)-O(2)		2.14×3	
Relative energy (eV/f.u.)			0.39		
Band gap (eV)			2.37		

tained β-Bi_2O_3 structure determined by a neutron-diffraction experiment.[35] β-Bi_2O_3 is known to be formed at 920 K during the cooling of δ-Bi_2O_3 (Ref. 7) or by the decomposition of $Bi_2O_2CO_3$ at 650 K.[35] The experimentally obtained transition enthalpy between α-Bi_2O_3 and β-Bi_2O_3 was reported to be 0.08 or 0.09 eV/f.u.[7,8] It is therefore natural that β-Bi_2O_3 appears in the present study as one of the lowest-energy forms. The experimental lattice parameters of β-Bi_2O_3 are a=7.739 and c=5.636 Å. The theoretical values are 3% and 1% larger than the experimental values, which are within the GGA error. The internal parameters are also in good agreement with each other. We can therefore identify the ⟨100⟩-LS(2×2×2) arrangement to be β-Bi_2O_3. The ⟨100⟩-LS(2×2×2) arrangement exhibits a band gap of 1.75 eV.

D. Symmetry breaking and local distortion in ⟨110⟩ array model

The same procedure as that described in the previous section is also carried out for ⟨110⟩ array model. The ⟨110⟩-HS arrangement has the strongest imaginary phonon frequency at the X point (1/2, 0, 0) shown in Fig. 4(b), which leads to the structure of the space group *Pmm*2 with a $\sqrt{2}\times 1/\sqrt{2}\times 1$ supercell as the unit cell. After the structure optimization with this space group, an imaginary frequency remains at the Y point (0, 1/2, 0). Optimization leads to another *Pmm*2 structure with a $\sqrt{2}\times\sqrt{2}\times 1$ supercell as the unit cell with a relative energy of 0.53 eV/f.u. and a band gap of 1.40 eV. However, the imaginary mode does not disappear. The procedure then requires a structure of the space group *Fmm*2 with a $2\sqrt{2}\times 2\sqrt{2}\times 2$ supercell as the unit cell. The calcula-

TABLE IV. Details of structure, Bi-O bond length, energy relative to α-Bi_2O_3, and band gap of ⟨111⟩-LS(2×2×2) arrangement of df-Bi_2O_3.

			⟨111⟩-LS(2×2×2)		
Space group			$Fd\bar{3}m$ (No. 227)		
Lattice parameter			a=11.41 Å		
Atom coordinate	Bi (1)	32*e*	0.370	0.370	0.370
	O (1)	48*f*	0.200	0	0
Bond length (Å)		Bi(1)-O(1)		2.14×3	
				2.86×3	
Relative energy (eV/f.u.)			0.29		
Band gap (eV)			2.59		

TABLE V. Details of structure, Bi-O bond length, energy relative to α-Bi_2O_3, and band gap of $\langle 100\rangle$-LS($2\times2\times2$) arrangement of df-Bi_2O_3.

			$\langle 100\rangle$-LS($2\times2\times2$)		
Space group			$P\bar{4}2_1c$ (No. 114)		
Lattice parameter			a=7.98 Å c=5.71 Å		
Atom coordinate	Bi (1)	8e	−0.029	0.261	0.247
	O (1)	4d	0	0.5	0.414
	O (2)	8e	0.321	0.288	−0.052
Bond length (Å)		Bi(1)-O(1)			2.14×1
		Bi(1)-O(2)			2.70×1 2.15×1 2.33×1 2.39×1 3.28×1
Relative energy (eV/f.u.)			0.08		
Band gap (eV)			1.75		

tion leads to a structure with a relative energy of 0.35 eV/f.u and a band gap of 1.83 eV. However, atomic displacements in this structure during the geometry optimization are too large for the position of the O atoms to be maintained in the $\langle 110\rangle$ array model. The imaginary mode does not disappear even in this model. Further symmetry-breaking calculations were not attempted. In conclusion, no dynamically stable arrangement for $\langle 110\rangle$ model within the $2\times2\times2$ supercell was found by the procedure adopted in the present study.

E. Symmetry breaking and local distortion in other array models of superstructures

Recently, several groups reported that other vacancy-array models with the $2\times2\times2$ superstructure exhibit lower energy than the three simple array models as described above. Two kinds of vacancy arrays of the superstructure are therefore studied in this section to search for low-energy arrangements. First, a bixbyite-type vacancy array is examined. The bixbyite structure is also called a C-rare-earth structure and is typical of sesquioxides such as Y_2O_3, In_2O_3, and Mn_2O_3. This structure belongs to the space group $Ia\bar{3}$ and can be considered as another vacancy-array model formed in the $2\times2\times2$ superstructure. The phonon band structure of the bixbyite-type Bi_2O_3 (bixbyite-HS) arrangement exhibits imaginary vibration modes. The symmetry breaking according to the imaginary mode at the H point (1, 0, 0) leads to the $Pa\bar{3}$ space group (bixbyite-LS) with a unit cell of the same size. The optimized structural data, bond length, energy, and band gap are summarized in Table VI for both HS and LS. The symmetry breaking reduces the energy to 0.07 eV/f.u., which is as low as the energy of β-Bi_2O_3. The low-energy structure that Aidhy *et al.*[17] reported has a space group of $Fm\bar{3}$, which can be classified into the bixbyite-type vacancy array in our terminology. This is the same array as that Music *et al.*[21] referred to as the combined $\langle 110\rangle$ and $\langle 111\rangle$ oxygen-vacancy ordering. Although they did not report the relative energy of their structures with respect to α-Bi_2O_3, their structures may be the same as the bixbyite-HS arrangement judging from the energy relative to other df-Bi_2O_3 arrangements. Mohn *et al.*[23] also reported a structure with the same vacancy array as this one, and referred to it as a $\langle 111\rangle+\langle 110\rangle$ structure. They reported many structures that have relative energies lower than the bixbyite-HS arrangement. However they clearly have higher energies than the bixbyite-LS arrangement found in the present study. Aidhy *et al.*[18] also suggested that their bixbyite-HS arrangement can be stabilized by including local distortion, although they have reported neither detailed structure nor energy gain after the structure optimization. The reported structure may be another local minimum structure within the bixbyite-type vacancy array. Although the polymorph that corresponds to the bixbyite-LS arrangement has not been reported experimentally, it is likely to be formed during the cooling of δ-Bi_2O_3, similar to the case of β-Bi_2O_3. We hereafter call the bixbyite-LS arrangement η-Bi_2O_3.

The second vacancy-array superstructure model considered is constructed by analogy to the orthorhombic Sb_2O_3 crystal known as valentinite. Note that the structure of valentinite belongs to the space group *Pccn*, which is the same as that of metastable ε-Bi_2O_3 reported in the literature.[9] This is a structure derived from the $\langle 100\rangle$ vacancy-array model. The unit cell with the [001] array is doubled in the [100] direction, which is accompanied by a translation of the vacancy array by half of the unit-cell parameter in the [010] direction. The highest-symmetry arrangement of this vacancy array has the space group *Ibam*, and it has an imaginary vibration mode at the Γ point (0, 0, 0). Following the procedure described above, the valentinite-LS arrangement

TABLE VI. Details of structure, Bi-O bond length, and energy relative to α-Bi_2O_3 of bixbyite-HS and -LS arrangements of df-Bi_2O_3.

	Bixbyite-HS					Bixbyite-LS				
Space group	$Ia\bar{3}$ (No. 206)					$Pa\bar{3}$ (No. 205)				
Lattice parameter	a=11.21 Å					a=11.42 Å				
Atom coordinate	Bi (1)	8*b*	0.25	0.25	0.25	Bi (1)	8*c*	0.255	0.255	0.255
	Bi (2)	24*d*	0.973	0	0.25	Bi (2)	24*d*	0.977	−0.009	0.259
	O (1)	48*e*	0.622	0.104	0.154	O (1)	24*d*	0.618	0.087	0.135
						O (2)	24*d*	0.104	0.636	0.681
Bond length (Å)	Bi(1)-O(1)		2.43×6			Bi(1)-O(1)		2.78×3		
						Bi(1)-O(2)		2.20×3		
	Bi(2)-O(1)		2.30×2			Bi(2)-O(1)		2.14×1		
			2.41×2					2.29×1		
			2.56×2					2.61×1		
						Bi(2)-O(2)		2.24×1		
								2.53×1		
								3.08×1		
Relative energy (eV/f.u.)	0.28					0.07				
Band gap (eV)	1.94					2.66				

with the space group *Pbcn* was obtained. The optimized structure data, bond length, relative energy, and band gap are summarized in Table VII. The valentinite-LS arrangement has a relative energy of 0.07 eV/f.u. and does not exhibit dynamical instabilities at any commensurate point. Since the space group of valentinite-LS is *Pbcn*, which is slightly different from that of ε-Bi_2O_3, *Pccn*, reported experimentally, the valentinite-LS arrangement is referred to as ε'-Bi_2O_3. Here is another example showing that the consideration of symmetry breaking and local distortion are essential.

TABLE VII. Details of structure, Bi-O bond length, and energy relative to α-Bi_2O_3 of valentinite-LS arrangement of df-Bi_2O_3.

	Valentinite-LS				
Space group	*Pbcn* (No. 60)				
Lattice parameter	a=11.81 Å b=5.74 Å c=5.69 Å				
Atom coordinate	Bi (1)	8*d*	0.128	0.309	0.550
	O (1)	4*c*	0	0.444	0.25
	O (2)	8*d*	0.715	0.090	0.112
Bond length (Å)	Bi(1)-O(1)			2.36×1	
				2.41×1	
	Bi(1)-O(2)			2.12×1	
				2.26×1	
				2.42×1	
				3.52×1	
Relative energy (eV/f.u.)	0.07				
Band gap (eV)	2.22				

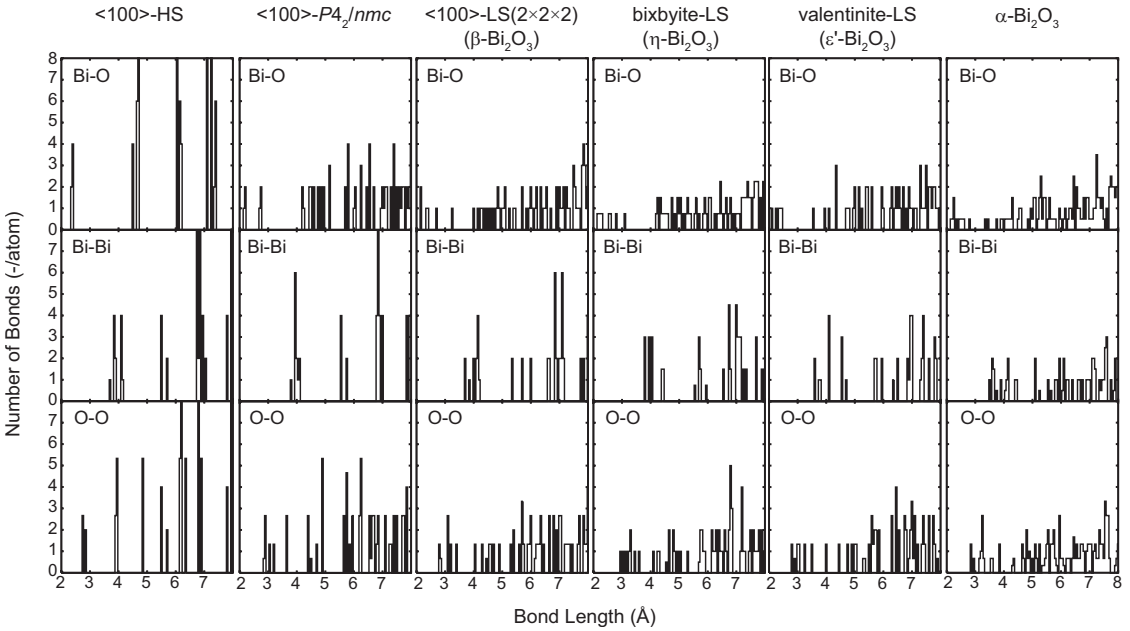

FIG. 7. Atomic pair distributions of Bi-O, Bi-Bi, and O-O in two high-symmetry arrangements of the ⟨100⟩ array, and those of the three stable arrangements of df-Bi_2O_3, and α-Bi_2O_3.

F. Magnitude of the zero-point vibration energy of four low-energy structures

Once the phonon-dispersion curves are obtained, one can evaluate the magnitude of the zero-point vibration energy (ZPE), E_{ZP}, for the given structure within the harmonic approximation. The vibrational density of states is found to be not significantly different between the three low-energy structures of df-Bi_2O_3 [⟨100⟩-LS($2\times2\times2$), bixbyite-LS, valentinite-LS] and α-Bi_2O_3. Consequently, E_{ZP} for the four structures are almost the same, ranging from 0.21 to 0.22 eV/f.u. In other words, the difference in the ZPE among the four structures is smaller than 0.01 eV/f.u. The contribution of the ZPE therefore does not change the energetic hierarchy of these structures.

IV. DISCUSSION

A. Atomic pair distribution in members of the df-Bi_2O_3 family

In the previous section, we reported that the symmetry breaking and local distortion are essential for obtaining dynamically stable and low-energy structures. To analyze the nature of the local distortion, the pair distributions for Bi-O, Bi-Bi, and O-O are examined. Figure 7 summarizes the results for the three low-energy structures in comparison with that for α-Bi_2O_3. To examine the effect of the symmetry breaking, results for higher-symmetry arrangements of the ⟨100⟩ array model, i.e., ⟨100⟩-HS and ⟨100⟩-$P4_2/nmc$, are compared with that for the ⟨100⟩-LS($2\times2\times2$) arrangement. It can be observed that the Bi-O pair distribution becomes evenly distributed upon lowering the symmetry, thereby lowering the energy. A similar tendency can be seen for the O-O pair distribution. On the other hand, the Bi-Bi pair distribution is less evenly distributed, even in the low-energy structures. The results imply that the symmetry breaking and local distortion have a larger impact on the O sublattice than on the Bi sublattice. In other words, the O sublattice is more vulnerable to the local distortion.

B. Electronic band gap of members of the df-Bi_2O_3 family

In experiments δ-Bi_2O_3 exhibits a clear band gap of 1.73 eV.[24] On the other hand, most previous theoretical calculations gave semimetallic or metallic electronic structures for the three simple arrays within the single unit cell of df-Bi_2O_3. We found that a clear band gap appears, even in the three vacancy-array models for df-Bi_2O_3, only when the local distortion is appropriately included. Figure 8 shows the relationship between the GGA band gap and the relative energy. There is a clear trend of the band gap decreasing with increasing relative energy for each vacancy array. The results imply that semimetallic or metallic electronic structures of

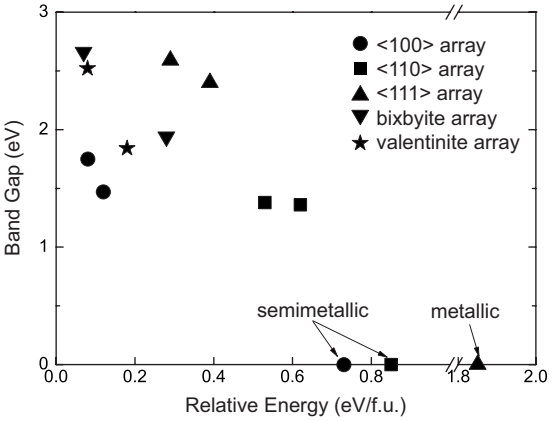

FIG. 8. Relation between band gap and energy relative to α-Bi_2O_3 for each vacancy-array model.

df-Bi_2O_3 are artifacts due to the selection of structures with too high energy to be realized under ordinary conditions.

C. Discussion on δ-Bi_2O_3 showing high oxide ionic conduction

Among the polymorphs of Bi_2O_3, δ-Bi_2O_3 is the only phase with high oxide ionic conductivity of more than 1 S/cm. A working hypothesis has been proposed that δ-Bi_2O_3 is the disordered phase in the df-Bi_2O_3 family and that the disordering plays a central role in the high oxide ionic conductivity. Experimentally, δ-Bi_2O_3 is known to be transformed to β-Bi_2O_3 during cooling. Although β-Bi_2O_3 is a member of the df-Bi_2O_3 family, it does not exhibit high oxide ionic conductivity. The $\delta-\beta$ transition at 923 K was found to be accompanied by a sudden change in the electrical conductivity and a transition enthalpy of 0.23 eV/f.u. The high intrinsic concentration of the vacant O sites alone cannot be a sufficient condition for the high oxide ionic conductivity.

Assuming that vacant sites in the O sublattice in δ-Bi_2O_3 is random, the primary contribution to the free-energy difference at the transition between δ and β is the configurational entropy, ΔS, which can be evaluated to be $\Delta S = -k_B(1/4 \ln 1/4 + 3/4 \ln 3/4) = 2.25 k_B$, where k_B is the Boltzmann constant. The contribution, $T\Delta S$, is 0.18 eV/f.u. at $T=923$ K, which is in reasonable agreement with the experimentally obtained transition enthalpy ΔH for $\delta-\beta$, i.e., $\Delta H = 0.23$ eV/f.u. at 923 K. On the basis of experimental data obtained by thermal analysis, Harwig and Gerards[7] reported that the degree of disorder in δ-Bi_2O_3, estimated by the relative entropy gain for the $\alpha-\delta$ transition, is comparable to that in liquid Bi_2O_3. These facts support the idea that δ-Bi_2O_3 is the disordered phase in the df-Bi_2O_3 family.

According to the present theoretical study, the three ordered phases, namely, β-Bi_2O_3 [$\langle 100\rangle$-LS($2\times2\times2$)], ε'-Bi_2O_3 (valentinite-LS), and η-Bi_2O_3 (bixbyite-LS), have relative formation energies of 0.07–0.08 eV/f.u., which is very close to the experimentally obtained transition enthalpy for $\alpha-\beta$, i.e., 0.08–0.09 eV/f.u.[7,10] Although neither the $\delta-\varepsilon'$ transition nor the $\delta-\eta$ transition has been experimentally observed, it may be possible to realize them under appropriate experimental conditions.

Since δ-Bi_2O_3 is the disordered phase, the configurational entropy should contribute to stabilizing δ-Bi_2O_3 at high temperatures. It is therefore essential to perform a statistical analysis of many different atomic arrangements to examine the phase stability and properties of δ-Bi_2O_3. A single DFT calculation of an ordered structure in the df-Bi_2O_3 family provide only limited information on δ-Bi_2O_3.

V. CONCLUSION

To search for a series of dynamically stable structures of df-Bi_2O_3, first-principles lattice dynamics calculations were systematically performed. Atomic arrangements were relaxed along imaginary modes of lattice vibrations in three vacancy-array models in the single unit cell and two vacancy-array models in the $2\times2\times2$ superstructure. The structures and energetics of low-energy structures were comprehensively discussed. The major results of this study can be summarized as follows: (1) within the $\langle 111\rangle$ array model, the $\langle 111\rangle$-LS($2\times2\times2$) arrangement was found to be dynamically stable with an energy of 0.29 eV/f.u. This arrangement is isostructural to arsenolite, As_2O_3, and senarmontite, Sb_2O_3. (2) Within the $\langle 100\rangle$ array model, the $\langle 100\rangle$-LS($2\times2\times2$) arrangement was found to be dynamically stable with an energy of 0.08 eV/f.u. This is identical to that of β-Bi_2O_3 obtained in experiments. (3) No dynamically stable arrangement for the $\langle 110\rangle$ array model within the $2\times2\times2$ supercell was found by the procedure adopted in the present study. The procedure eventually led to a structure that cannot be included in the $\langle 110\rangle$ array model. (4) Two other vacancy-array models with the $2\times2\times2$ superstructure were examined. A bixbyite-LS arrangement was found to be dynamically stable with an energy of 0.07 eV/f.u. Although no polymorph corresponding to this arrangement has been reported experimentally, it may be possible to form it under appropriate experimental conditions. We call this phase η-Bi_2O_3. (5) Within the valentinite-array model with the $2\times2\times2$ superstructure, the valentinite-LS arrangement was found to be dynamically stable with an energy of 0.07 eV/f.u. The vacancy array of valentinite-LS is the same as that of ε-Bi_2O_3, which was reported experimentally. Since the space group of valentinite-LS is different from that of ε-Bi_2O_3 reported experimentally, we call the phase ε'-Bi_2O_3. (6) The distribution of atom pairs in low-energy models was examined. The symmetry breaking and local distortion have a larger impact on the O sublattice than on the Bi sublattice. Both Bi-O and O-O pair distributions become evenly distributed upon lowering the symmetry, thereby lowering of energy. (7) In most previous theoretical calculations, semimetallic or metallic electronic structures were obtained for the three vacancy-array models within the single unit cell of df-Bi_2O_3. We found that a clear band gap appears in these arrangements only when the local distortion is appropriately included. There is a clear trend of the band gap decreasing with increasing relative energy. (8) β-Bi_2O_3, ε'-Bi_2O_3, and η-Bi_2O_3 are suggested to be ordered low-temperature polymorphs of the disordered δ-Bi_2O_3 in the df-Bi_2O_3 family. The relative energy of β-Bi_2O_3 obtained by the present calculation agrees with the experimental transition enthalpy, ΔH, for $\alpha-\beta$, which can be ascribed to the entropy term, $T\Delta S$, at the transition.

ACKNOWLEDGMENTS

This study was supported by both a Grant-in-Aid for Scientific Research (A) and a Grant-in-Aid for Scientific Research on Priority Areas "Nano Materials Science for Atomic Scale Modification 474" from the Ministry of Education, Culture, Sports, Science and Technology (MEXT) of Japan. A.M. thanks the Japan Society for the Promotion of Science.

*matsumoto@cms.mtl.kyoto-u.ac.jp
†y.koyama@at7.ecs.kyoto-u.ac.jp
‡tanaka@cms.mtl.kyoto-u.ac.jp

[1] M. Drache, P. Roussel, and J. Wignacourt, Chem. Rev. **107**, 80 (2007)..
[2] N. M. Sammes, G. A. Tompsett, H. Näfe, and F. Aldinger, J. Eur. Ceram. Soc. **19**, 1801 (1999)..
[3] L. G. Sillen, Ark. Kemi **12A**, 1 (1937).
[4] V. G. Gattow and H. Schröder, Z. Anorg. Allg. Chem. **318**, 176 (1962)..
[5] V. G. Gattow and D. Schutze, Z. Anorg. Allg. Chem. **328**, 44 (1964)..
[6] E. M. Levin and R. S. Roth, J. Res. Natl. Bur. Stand. **68A**, 197 (1964).
[7] H. A. Harwig and A. G. Gerards, Thermochim. Acta **28**, 121 (1979)..
[8] C. N. R. Rao, G. V. S. Rao, and S. Ramdas, J. Phys. Chem. **73**, 672 (1969)..
[9] N. Cornei, N. Tancret, F. Abraham, and O. Mentré, Inorg. Chem. Commun. **45**, 4886 (2006).
[10] A. F. Gualtieri, S. Imovilli, and M. Prudenziati, Powder Diffr. **12**, 90 (1997).
[11] T. Takahashi, H. Iwahara, and Y. Nagai, J. Appl. Electrochem. **2**, 97 (1972)..
[12] P. D. Battle, C. R. A. Catlow, J. Drennan, and A. D. Murray, J. Phys. C **16**, L561 (1983)..
[13] M. Yashima and D. Ishimura, Chem. Phys. Lett. **378**, 395 (2003)..
[14] N. I. Medvedeva, V. P. Zhukov, V. A. Gubanov, D. L. Novikov, and B. M. Klein, J. Phys. Chem. Solids **57**, 1243 (1996)..
[15] J. M. Carlsson, B. Hellsing, H. S. Domingos, and P. D. Bristowe, Phys. Rev. B **65**, 205122 (2002)..
[16] A. Walsh, G. W. Watson, D. J. Payne, R. G. Edgell, J. Guo, P. Glans, T. Learmonth, and K. E. Smith, Phys. Rev. B **73**, 235104 (2006)..
[17] D. S. Aidhy, J. C. Nico, S. B. Sinnott, E. D. Wachsman, and S. R. Phillpot, J. Am. Ceram. Soc. **91**, 2349 (2008)..
[18] D. S. Aidhy, S. B. Sinnott, E. D. Wachsman, S. R. Phillpot, and J. C. Nino, J. Solid State Chem. **182**, 1222 (2009)..
[19] G. Zhong, J. Wang, and Z. Zeng, Phys. Status Solidi B **245**, 2737 (2008)..
[20] G. Zhong, Y. Wang, Z. Dai, J. Wang, and Z. Zeng, Phys. Status Solidi B **246**, 97 (2009)..
[21] D. Music, S. Konstantinidis, and J. M. Schneider, J. Phys.: Condens. Matter **21**, 175403 (2009)..
[22] C. E. Mohn, S. Stølen, S. T. Norberg, and S. Hull, Phys. Rev. Lett. **102**, 155502 (2009)..
[23] C. E. Mohn, S. Stølen, S. T. Norberg, and S. Hull, Phys. Rev. B **80**, 024205 (2009)..
[24] H. T. Fan, S. S. Pan, X. M. Teng, C. Ye, and G. H. Li, J. Phys. D **39**, 1939 (2006)..
[25] P. Blöchl, Phys. Rev. B **50**, 17953 (1994)..
[26] G. Kresse and J. Hafner, Phys. Rev. B **47**, R558 (1993)..
[27] G. Kresse and J. Furthmuller, Phys. Rev. B **54**, 11169 (1996)..
[28] G. Kresse and J. Furthmuller, Comput. Mater. Sci. **6**, 15 (1996)..
[29] J. P. Perdew, K. Burke, and M. Ernzerhof, Phys. Rev. Lett. **77**, 3865 (1996)..
[30] A. Togo, http://fropho.sourceforge.net/.
[31] A. Togo, F. Oba, and I. Tanaka, Phys. Rev. B **77**, 184101 (2008)..
[32] A. Togo, F. Oba, and I. Tanaka, Phys. Rev. B **78**, 134106 (2008)..
[33] S. A. Ivanov, R. Tellgren, H. Rundlof, and V. G. Orlov, Powder Diffr. **16**, 227 (2001)..
[34] T. P. Debies and J. W. Rabalais, Chem. Phys. **20**, 277 (1977)..
[35] S. K. Blower and C. Greaves, Acta Crystallogr., Sect. C: Cryst. Struct. Commun. **44**, 587 (1988)..